AIAA 80-0286R

Correlation of Nosetip Boundary-Layer Transition Data Measured in Ballistics-Range Experiments

Daniel C. Reda*
Sandia National Laboratories, Albuquerque, N. Mex.

Preablated nosetips of various carbonaceous materials were tested in a ballistics range. Surface-temperature contours, measured with image-converter cameras, were used to define boundary-layer transition-front contours. Measurements of surface roughness, surface temperature, average transition-front location, and freestream environment were combined with calculations of nosetip flowfields, and with calculations of laminar boundary-layer development in these flowfields, to transform all data into various dimensionless parameters. These parameters were defined by previous attempts to correlate existing wind-tunnel data for transition on rough/blunt bodies. Of the available correlating techniques, only one, based on the concept of a constant (critical) roughness Reynolds number for transition, was found to successfully describe both the wind-tunnel and ballistics-range data, thereby validating the extrapolation of this concept to actual re-entry vehicle materials and environments.

Nomenclature

a	= coefficient of disturbance parameter
D	$= 2R_N$
h	= measured in-plane roughness element height
$\bar{h}$	= arithmetic average of h distribution
h'	= defined by Eq. (1)
k	= physical peak-to-valley roughness element height
$\bar{k}$	= arithmetic average of k distribution
M	= Mach number
n	= exponent of disturbance parameter
P	= pressure
PE	= probability of exceedence
Re	= Reynolds number, $\rho U/\mu$
R_N	= nosetip radius
S	= arc length, measured from stagnation point
T	= temperature
(T'/T_e)	= denominator of transition parameter given in Eqs. (5)
U	= velocity
X	= disturbance parameter
Y	= transition parameter
θ	= momentum thickness
μ	= viscosity
ν	= kinematic viscosity, μ/ρ
ρ	= density
σ	= standard deviation

Subscripts

D	= based on D
e	= at boundary-layer edge
h	= of, or based on, h distribution
k	= based on conditions at k
S	= based on S
TR	= at transition
w	= at wall
θ	= based on θ
∞	= freestream
0.95, 0.05	= 95, 5% of all roughness elements possess values greater than this

Presented as Paper 80-0286 at the AIAA 18th Aerospace Sciences Meeting, Pasadena, Calif., Jan. 14-16, 1980; submitted March 11, 1980; revision received Sept. 15, 1980. Copyright © American Institute of Aeronautics and Astronautics, Inc., 1980. All rights reserved.

*Member, Technical Staff, Fluid and Thermal Sciences Department. Associate Fellow AIAA.

I. Introduction

VIABLE techniques for predicting and improving the accuracy of ballistic re-entry vehicles have been actively pursued in recent years. It has now been established that asymmetric nosetip shape change is one of the most influential factors in re-entry generated contributions to overall strategic-system inaccuracies (e.g., see results of Refs. 1-4). Aerodynamic forces and moments that act directly on asymmetrically-ablated nosetips, and associated flow distortions that these shapes impose on otherwise axisymmetric afterbody flowfields, can result in re-entry body trim growth (angle-of-attack), and possible roll-rate excursions, creating a dispersion of the re-entry vehicle from its predicted ballistic impact point.

Carbonaceous nosetip materials, both graphites and carbon/carbon composites, sublime under high altitude laminar-flow conditions, forming a surface microroughness distribution characteristic of each material's composition and fabrication/processing technique. Surface roughness element heights typically span at least an order of magnitude and can thus only be represented in a statistical sense (as will be demonstrated in Sec. II). Surface microroughness elements, as formed during re-entry, create disturbances within the laminar boundary layer; as altitude decreases, Reynolds number increases, and nosetip flowfield conditions capable of amplifying these roughness-induced disturbances are eventually achieved, i.e., transition onset occurs. Boundary-layer transition to turbulence results in more severe heat-transfer rates, increased ablation rates, accelerated shape change, and the formation of a macroroughness pattern downstream of transition (e.g., striations, grooves, and/or scallops) which further augment the turbulent convective heat transfer rates.

Based on present understanding, transition initially occurs on the nosetip in the vicinity of the sonic line, $(S/R_N) \sim 0.7$, and progresses forward at a rate dependent on both the material surface roughness and the re-entry vehicle trajectory. Under some conditions, this forward progression occurs rapidly, and a rather symmetric/biconic nosetip shape results. However, under conditions where the leading edge of the transition zone remains removed from the stagnation point throughout any appreciable portion of the trajectory, a laminar island forms, followed by an indented/turbulent-flow region.

Since the surface microroughness distribution is statistical in nature, transition must be described (modeled) in a probabilistic sense, i.e., there exists a probability that transition will occur at a specified distance along each ray emanating from the nosetip stagnation point. Asymmetric

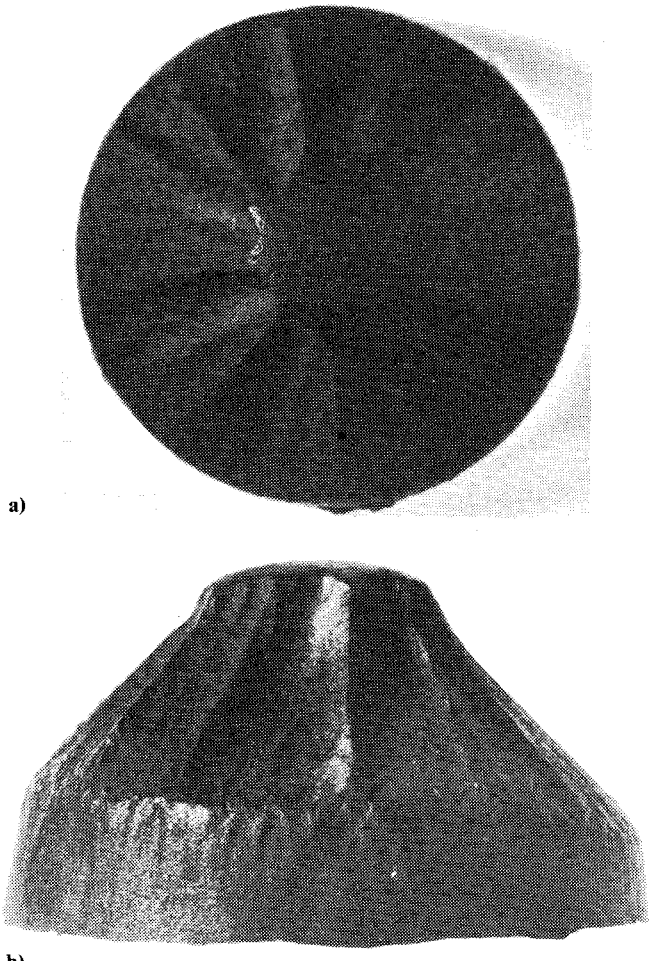

a)

b)

Fig. 1 NRV nosetip.

transition fronts thus result, and are the driving potential for asymmetric nosetip shape change.

Figure 1 shows an example of an asymmetric nosetip shape that illustrates these points. It was formed during a re-entry flight test of an initially hemispherical graphite nosetip.[1]

A procedure for the calculation of asymmetric nosetip shape change during re-entry, based on the above-described phenomenological arguments, was recently formulated by Dirling.[2] This procedure, when mathematically coupled with predictions of resulting vehicle aerodynamics,[3,4] allows for the probabilistic calculation of re-entry body trim growth on any specified trajectory. A statistically large number of computer runs could be made for each of several trajectories bracketing a missile system's operating envelope, thereby analytically defining nosetip-induced contributions to the system's overall circular-error probability. Further, such an exercise could be conducted for a total cost significantly below that of even a single flight test.

As promising as such a technique appears, certain key elements in the procedure remain to be proven. Of critical importance is the "transition law" utilized. Obviously, for nosetip shape-change history to be accurately predicted, a code must realistically model transition onset, average (or mean) transition-front location, and the statistics of the transition-front contour about its predicted mean location, as a function of the ablated material surface roughness characteristics and the laminar boundary-layer development up to transition.

During the first half of the 1970's, the re-entry community relied heavily on two primary data sources for the generation of correlations aimed at modeling transition onset/location on re-entry vehicle nosetips.[5,6] These data were obtained on nonporous, metallic, thin-skin calorimeter models, of various uniform surface roughness scales, exposed to Mach 5 and Mach 8 ideal-gas wind-tunnel environments. No information concerning the asymmetric nature of transition was obtained.

More recently conducted wind-tunnel experiments yielded extensions to the above-noted data base: Laderman[7] and Demetriades[8] examined the separate and combined influences of roughness and blowing on nosetip boundary-layer transition at Mach 6, while Demetriades[9] further studied the effects of distributed sandgrain roughness on blunt-body transition (without blowing) as simulated by the boundary-layer flow on the converging-diverging wall of a wind-tunnel nozzle.

Based primarily on the data of Refs. 5 and 6, Anderson,[5] Dirling,[10] Van Driest[11] (comments which evolved from work reported in Refs. 12 and 13), Finson,[14] and Bishop[15] all formulated semiempirical correlations for nosetip boundary-layer transition; each of these correlations well described the available wind-tunnel data. What remained to be determined, therefore, was the validity of extrapolating such correlations to the prediction of mean transition-front locations on actual nosetip materials/geometries exposed to hypersonic real-gas environments. Empirical information on the asymmetric nature of transition-fronts on ablating graphite and carbon/carbon nosetips was also required.

Toward these ends, ballistics-range nosetip-transition experiments were conducted utilizing three bulk graphite and two carbon/carbon composite nosetip materials.[16-20] It is the objective of the present paper to combine these published experimental results with computations of nosetip flowfields, and with computations of laminar boundary-layer development in these flowfields, in order to validate existing correlations, or, failing that, to formulate a viable alternative for use in nosetip shape-change codes.

II. Review of Experimental Techniques

The purpose of this section is to very briefly summarize the methods and techniques utilized in the acquisition of the ballistics-range nosetip-transition data base. More detailed information on these subjects is given in Refs. 16-20.

Five nosetip materials were tested. The three bulk graphites included a coarse-grain graphite ATJ-S, an intermediate-grain-size graphite CMT, and a fine-grain graphite Graphnol (GNOL); the two woven materials were a fine-weave-pierced-fabric (FWPF) and a 223 weave carbon/carbon (223 C/C).

All nosetips were preablated in a low-pressure, high-enthalpy, arc-jet environment in order to create the proper initial condition (characteristic laminar microroughness) for each material prior to launch. At least one nosetip of each material tested was sectioned and the laminar microroughness distribution defined via microscopy (see Figs. 2 and 3).

From a surface-roughness viewpoint, bulk graphites are, by far, the "simplest" nosetip materials to characterize, consisting solely of grains and binder material. In Ref. 20, it was noted that average graphite surface-roughness height scaled linearly with average grain size for the three bulk graphites incorporated herein.

For each woven material, roughness element heights were measured on the ablation-exposed surfaces of its three constituents: axial fiber ends, transverse fiber surfaces, and matrix or filler-material surfaces. Constituent surface roughness element height distributions were then mathematically weighted, based on the exposed surface-area fraction of each constituent and its associated number of roughness elements per unit surface area, to form an overall or "composite" microroughness distribution. Such a technique does not include any description of the larger-scale surface roughness pattern that forms due to differential ablation (recession) between these various constituents (recall discussions in Ref. 20). Obviously, such materials possess inherently complex, three-dimensional, surface roughness patterns and any attempts to quantify them by a "composite-

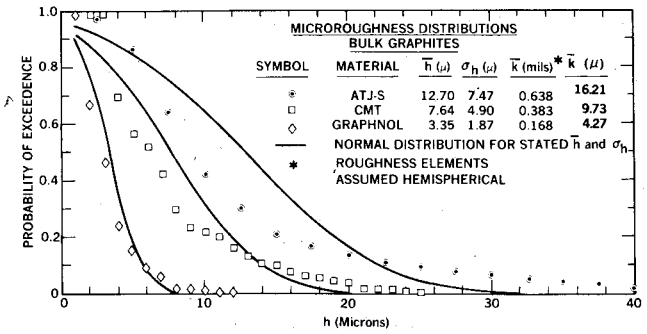

Fig. 2 Microroughness distributions, bulk graphites.

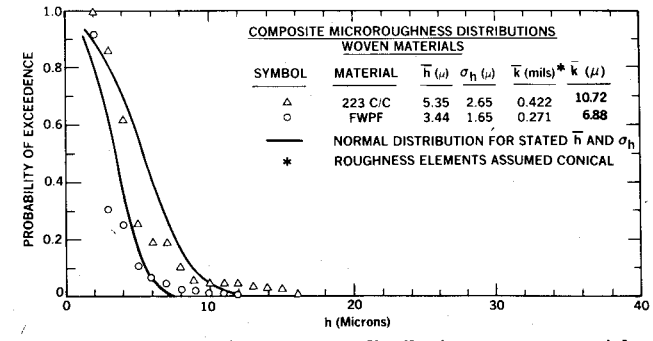

Fig. 3 Composite microroughness distributions, woven materials.

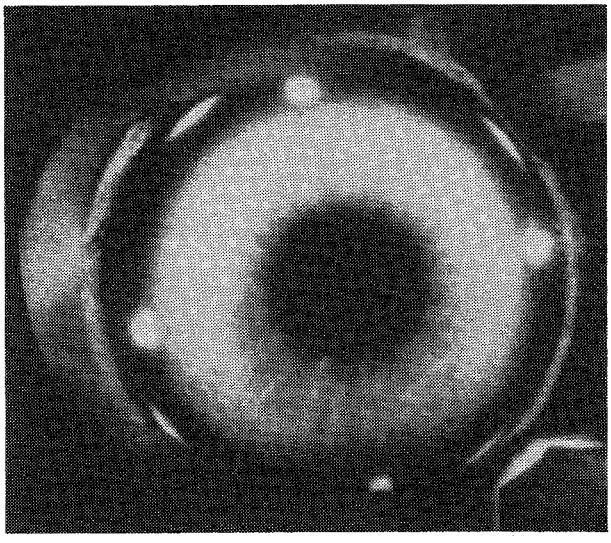

Fig. 4 Typical image—converter—camera photograph.

averaging technique" may be subject to question. Further discussions on this topic will be presented in Sec. III.

All remaining preablated nosetips were mounted on ballistics-range models and launched at hypersonic velocity into well-defined clear-air environments. With the exception of the ATJ-S experiments, all tests were conducted on track-G at the Arnold Engineering and Development Center.[21]

Nosetip surface-temperature contours were measured along each range trajectory with image-converter cameras (Fig. 4 shows a typical data negative). Results were interpreted with interactive graphics in order to define nosetip transition-front contours. An $(S/R_N)_{TR}$ value along any given ray was defined by the physical location where the surface temperature curve underwent a positive change in slope, the locus of all such points defining the transition-front contour. A mean transition-front location was calculated for each data-acquisition station simply by arithmetically averaging the $(S/R_N)_{TR}$ values measured along individual rays emanating from the nosetip stagnation point.

Measurements of nosetip surface roughness, surface temperature, average transition-front location, and freestream environment were then combined with calculations of nosetip flowfields, and with calculations of laminar boundary-layer development in these flowfields, in order to transform all data into the coordinates utilized in the correlations of Refs. 5, 10, 11, 14, and 15.

III. Results

Prior to showing any comparisons of present experimental results with existing nosetip transition correlations, several key points will be addressed and several experimental observations reiterated.

To initiate these discussions, Fig. 5 is introduced. This schematic serves to summarize the general framework into which all nosetip transition correlations have been cast. Further, it provides a basis from which to describe the physical picture that has emerged concerning roughness-dominated transition on blunt bodies.

As noted earlier, laminar ablation at high altitude causes surface roughness elements to form. These roughness elements are the primary disturbance generators within the laminar boundary layer.

The problem then becomes to quantify the disturbance-generation capability of a given surface-roughness pattern. In all correlations formulated to date, attempts to meet this requirement were made by introducing a surface-roughness height scale into the disturbance parameter term X, coupled with one or more fluid-mechanic and/or geometric variables. Surface-roughness patterns have thus always been quantified by a single number (some average or maximum peak-to-valley roughness height); no measure of the roughness-element spacing or periodicity has yet to be introduced. Such a modeling approach seems entirely justified for the "sand-grain-like" surface-roughness patterns of the bulk graphites, but, in all probability, represents a serious deficiency in attempts to describe the complex, three-dimensional, surface-roughness patterns formed on the woven materials. Additional discussions of this issue will be given shortly.

The dependent variable Y is here referred to as the transition parameter which, in all cases considered, contains only fluid-mechanic and geometric quantities; it serves to define the response of the laminar boundary layer to various levels of disturbance inputs. A power-law relationship between Y_{TR} and X was derived in each correlation under review (for a complete tabulation of all results, see Ref. 30).

For "large" values of the disturbance parameter, transition occurs "early," while for "small" values it occurs "later." Two experimental observations resulting from ballistics-range testing support this general view:

1) For a given roughness distribution (nosetip material), as the range static pressure was increased (i.e., as the freestream Reynolds number was increased), the average transition-front location progressed forward, closer to the nosetip stagnation point.

2) For a constant flow environment, within each class of materials tested (graphites and carbon/carbon composites) correlation was found to exist between the postulated disturbance source (average, or composite average, microroughness element height) and the laminar boundary-layer response (average transition-front location). As roughness height was increased, transition occurred closer to the nosetip stagnation point.

Consistent with practices used in the correlations under review, "smooth-wall"/laminar-boundary-layer computations were used to generate required profile parameters for all transition correlations except Finson's. In fact, under present test conditions ($\bar{k}/\theta \leq 3.5$), Finson's calculations showed little or no effect of surface roughness on laminar boundary-layer development. Consequently, the code of Ref.

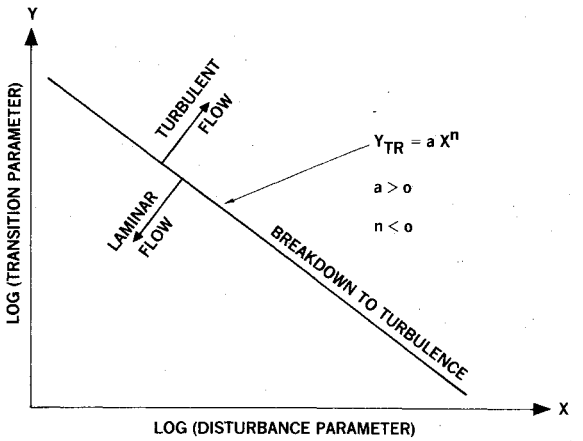

Fig. 5 Generalized correlation approach applied to nosetip transition data.

22 was used to compute smooth-wall laminar boundary-layer edge and integral profile parameters for transformation of present data into coordinates utilized in Refs. 5, 11, and 15. Transformations requiring computations of laminar boundary-layer profiles[10,14] were accomplished by Dirling and Finson and supplied to the present author.

The surface-roughness-quantification issue will now be addressed in more detail. As was noted earlier in this section, average and composite-average surface roughness heights were used to characterize the disturbance-generation capability of each graphitic and woven material, respectively.

Surface roughness characterization via microscopy dictates that individual surface roughness elements be viewed and measured in a cross-sectioned plane, i.e., in two dimensions (recall Figs. 2 and 3). Actual surface roughness elements are, of course, three dimensional. A transformation of these planar measurements to physical peak-to-valley dimensions is thus required. Dirling[23] has discussed this issue in some detail.

Basically, while it is possible to transform an entire h distribution into its corresponding k distribution, the required mathematical manipulations are rather complex; transformation of a given $\bar{h}$ value to its corresponding $\bar{k}$ value is, on the other hand, straightforward.

The analysis approach that has evolved, therefore, is one which attempts to relate average roughness height to average transition-front location. A separate, empirical definition of transition-front asymmetry, as a function of mean transition-front location can then be generated for any material of interest using present experimental techniques (e.g., the CMT graphite results of Ref. 19). Further substantiation for this approach is noted below.

It has been argued in the past that perhaps the largest 10 to 20% of all roughness elements in a given distribution dominate the transition process. Along these lines, if one takes the h distributions of Figs. 2 and 3 are replots them in terms of a nondimensional height scale

$$h' = [h - h_{0.95}]/[h_{0.05} - h_{0.95}] \tag{1}$$

then all five distributions are seen to collapse to a single band described by the exponential relationship

$$\mathrm{PE}\,(\pm 20\%) = 0.95\,(10)^{-1.2788h'} \tag{2}$$

The ratio of any percentile value of h to its corresponding $\bar{h}$ was found to be essentially constant for all materials considered. For data-correlation purposes, uniformly increasing the roughness height scale of all five materials by a constant multiplier would not be expected to alter any of the conclusions reached herein.

A third experimental observation and its implications are now reiterated[20]:

3) For a given flow environment, consistency of results between the two classes of materials was not achieved, i.e., when measured mean transition-front locations were plotted vs average microroughness heights for the graphites, and vs composite average microroughness heights for the orthogonal-weave composite materials, two separate but essentially parallel curves resulted.

In essence, this experimental observation says that if one chooses to define the disturbance-generation capability of any woven-material surface-roughness pattern by a single parameter, namely, by its composite-average microroughness element height, then a separate nosetip transition correlation will be required for each class of materials (one for bulk graphites, one for orthogonal-weave composite materials, etc.). The physical reason behind this observation stems from the fact that the tripping effectiveness of a surface-roughness pattern is a function not only of the roughness-element heights, but also of the roughness-element shapes and spacings. This result was clearly shown by Smith and Clutter[24] some twenty years ago. Laderman's more recent results,[7] obtained on a blunt body in supersonic flow, further substantiated these early results; his experiments showed that a woven/wire-screen overlay of a given roughness height was more effective at tripping the boundary layer than a uniform sand-grain roughness pattern of an equivalent height. Essentially the same result was found during present experiments, namely, for a specified composite-average roughness height, the woven materials were inherently more effective at tripping the laminar boundary layer to a turbulent state when compared to bulk graphites of an equivalent average roughness height.

What is desired, however, is a unified (single) correlation valid for predicting transition locations on all carbonaceous nosetips regardless of material fabrication techniques.

A similar "roughness-effects" problem was encountered for turbulent boundary-layer flows over rough surfaces: how could one define the influence of any complex, two-, or three-dimensional surface-roughness pattern on turbulent boundary-layer velocity profiles and associated surface shear-stress levels in a unified way?

The approach that evolved there was to experimentally measure the "response" of the turbulent boundary layer to a given surface roughness pattern and then to "compare" this response (defined as the shift in the velocity profile due to surface roughness, when plotted in law-of-the-wall coordinates) to those observed for identical flows over sand-grain roughness patterns.[25] In this way, an "equivalent sand-grain roughness" could be defined for any complex surface-roughness pattern, making subsequent analyses in terms of this single equivalent sand-grain roughness height straightforward (i.e., the method provided a technique to characterize the effectiveness of any complex surface roughness pattern by a single roughness height scale).

The problem encountered in the present case is quite similar in that we wish to characterize, for each woven material, the tripping effectiveness of a complex, three-dimensional, surface-roughness pattern in terms of a single roughness height scale.

What is required, therefore, is to expose each woven material to a given flow environment and measure the response of the laminar boundary layer (average transition-front location) to the specific surface-roughness pattern. An extensive data base for bulk graphites must also be established to experimentally define the tripping effectiveness of basic sand-grain-like surface-roughness patterns under identical flow conditions. The graphite data base then provides the basis for comparison.

In practice, one could then empirically define the "equivalent mean graphitic microroughness height" of any woven-material surface-roughness pattern by noting the shift required to collapse the woven-material data onto the bulk-

graphite data, both plotted in the same disturbance-parameter, transition-parameter coordinates.

This approach was applied to the two woven materials tested under the present effort. For all correlations (coordinates) considered, the woven materials were found to posses equivalent mean graphitic microroughness heights double those values defined by the composite-average technique.

Table 1 summarizes the surface-roughness values used in present data analyses and also serves as a symbol key for all graphical comparisons to follow.

A. Passive Nosetip Technology Correlation

Anderson's analysis[5] of the Passive Nosetip Technology (PANT) wind-tunnel data base resulted in the transition correlation summarized by Eqs. (3):

$$Re_{\theta,\mathrm{TR}} = 215\left[\frac{k}{\theta}\frac{T_e}{T_w}\right]^{-0.7} \tag{3a}$$

where

$$Re_\theta\left[\frac{k}{\theta}\frac{T_e}{T_w}\right]^{0.7} \geq 255 \quad \text{by } M_e = 1.0 \tag{3b}$$

The empirically-defined disturbance parameter was shown in Ref. 5 to correlate with the relative kinetic energy at the top of the roughness elements, $\rho_k U_k^2/\rho_e U_e^2$, which was hypothesized to be the key physical measure of roughness-generated disturbances. The disturbance parameter noted in Eqs. (3) was used, however, due to the lack of any predictive capability in the then-existing nosetip shape-change codes for boundary-layer profile quantities such as ρ_k and U_k. The transition parameter was taken to be Re_θ.

Results of the PANT wind-tunnel experiments showed transition to always occur upstream of the sonic-line location, which led to the requirement noted in Eqs. (3). The physical basis for this requirement was felt to rest with two stabilizing influences known to be present but not explicitly included in Eqs. (3), namely, the favorable streamwise pressure gradient and the normal pressure gradient (across the boundary layer), both associated with flow over a convex surface.

Figure 6 shows a comparison of present data with the PANT correlation. Here, as in all cases to follow, the ballistics-range data set was subjected to a linear least-squares fit (in logarithmic coordinates) in order to define its corresponding coefficient a and exponent n. The resulting equation was then represented graphically by a solid line, with dashed lines above and below it to illustrate ±20% variations in the transition-parameter coordinate. The equation used to define each transition-location correlation under review was plotted in an identical manner.

Data for three different nosetip radii and five different nosetip materials collapsed to a reasonable band in PANT coordinates but showed a much stronger dependence ($n = -1.30$) of transition location on the postulated disturbance parameter vs that predicted by PANT ($n = -0.70$). A crossover within the cycle of interest to re-entry environments ($1 \leq (k/\theta)(T_e/T_w) \leq 10$) was also witnessed.

Previous ballistics-range transition experiments conducted under conditions where surface-roughness and pressure-gradient effects were absent[26] showed a strong dependence of transition Reynolds number on unit Reynolds number. Figure 7 shows a similar plot for present data, with surface roughness held constant (i.e., for a given material, here CMT graphite). The edge unit Reynolds number at transition was found to be constant over a regime in which the transition Reynolds number, based on edge properties and wetted run length, increased by an order of magnitude!

Expanding this observation further, all ballistics-range data were plotted as $Re_{\theta,\mathrm{TR}}$ vs (k/θ) in logarithmic coordinates (see Fig. 8). A curve fit of these results yielded $a = 106$, $n = -1.03$, i.e.,

$$[\rho_e U_e \theta/\mu_e]_{\mathrm{TR}} = 106(\bar{k}/\theta)^{-1.03} \tag{4a}$$

or

$$[\rho_e U_e \bar{k}/\mu_e]_{\mathrm{TR}} \cong 106 \cong \text{const} \tag{4b}$$

It was noted in Ref. 5 that the distribution of $Re_\theta[(k/\theta)(T_e/T_w)]^{0.7}$ with (S/R_N) around a nosetip was quite similar to the distribution of $[\rho_e U_e k/\mu_e]$, both monotonically increasing from zero at the stagnation point to maximum values at the sonic-line location, followed by a drop off to levels existing on the conic frustum of the afterbody. The first of these parameters, however, was found to better correlate the wind-tunnel data. Thus the concept of a constant (critical) roughness Reynolds number for transition, based on edge properties and average roughness height, does not reconcile these two independent data sets. Modifications of this fundamental idea will ultimately be shown herein to

Table 1 Summary of data symbols and material microroughness values

SYM	MAT	R_N cm	R_N in	$\bar{k}$ microns	$\bar{k}$ mils
○	CMT	1.02	0.4	9.73*	0.383*
◑	CMT	2.29	0.9	9.73*	0.383*
●	CMT	3.18	1.25	9.73*	0.383*
□	ATJ-S	1.02	0.4	16.21*	0.638*
◇	GNOL	1.02	0.4	4.27*	0.168*
△	FWPF	1.02	0.4	13.77**	0.542**
▲	FWPF	2.29	0.9	13.77**	0.542**
○	223 C/C	1.02	0.4	21.44**	0.844**
◑	223 C/C	2.29	0.9	21.44**	0.844**

*HEMISPHERICAL ELEMENTS ASSUMED

**CONICAL ELEMENTS ASSUMED; COMPOSITE AVERAGE DOUBLED

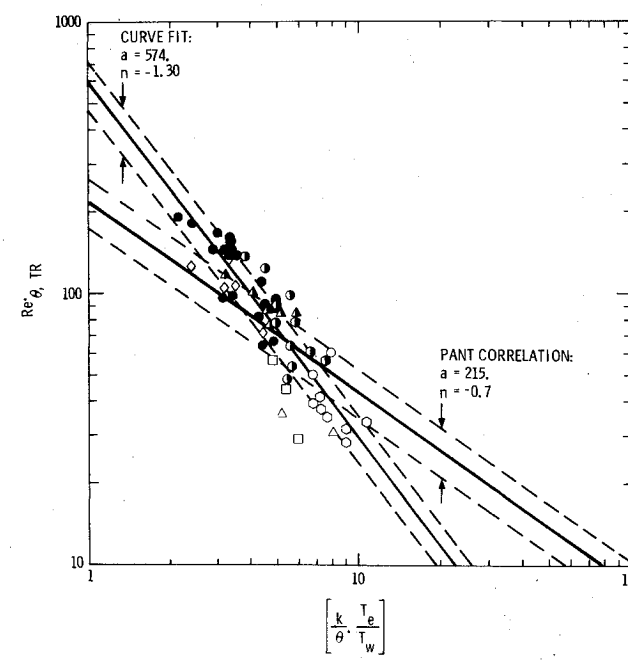

Fig. 6 Ballistics-range data vs PANT correlation.

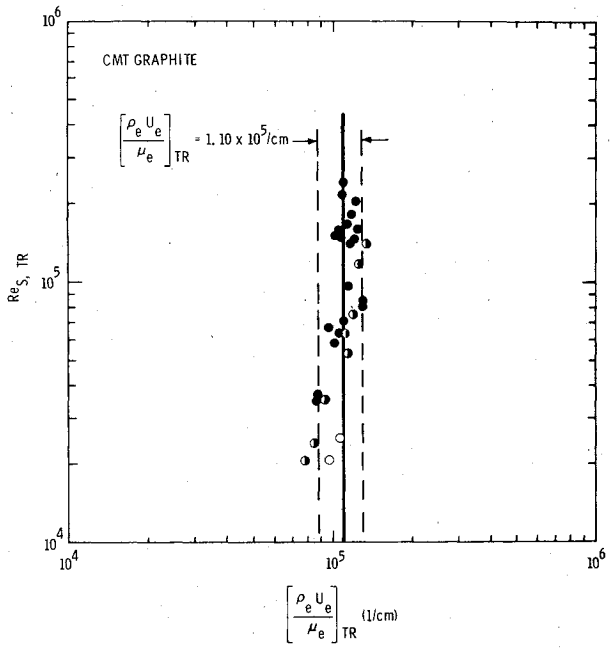

Fig. 7 Transition Reynolds number vs unit Reynolds number, CMT graphite data.

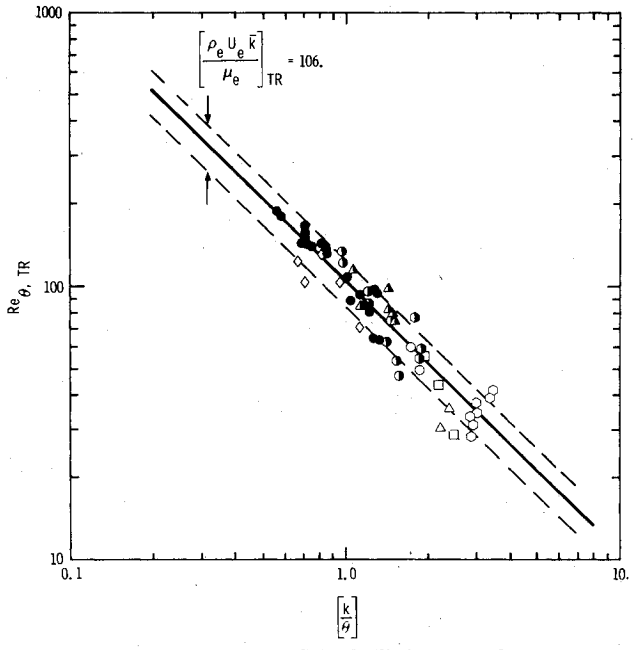

Fig. 8 $Re_{\theta,\mathrm{TR}}$ vs (k/θ) for ballistics-range data.

achieve this desired goal, namely a unified description of both data sets.

B. Van Driest Correlation

Van Driest,[11] based on his previous experimental observations and analyses,[12,13] offered technical comments on the PANT correlation. A modified correlation resulted, as described by Eqs. (5)

$$\frac{Re_{\theta,\mathrm{TR}}}{\left[1+0.9\left(\frac{T_w}{T_e}-1\right)+0.048M_e^2\right]_{\mathrm{TR}}}=200\left[\frac{k/\theta}{1+350\left(\frac{k}{R_N}\right)}\right]^{-1} \tag{5a}$$

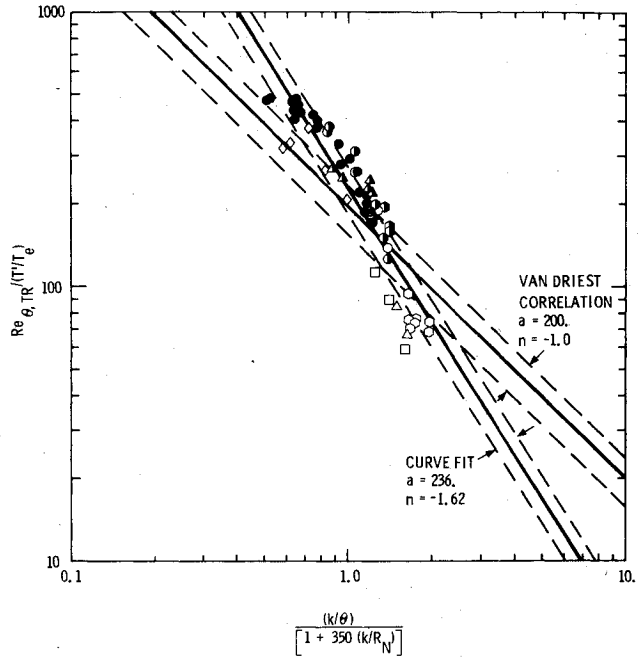

Fig. 9 Ballistics-range data vs Van Driest correlation.

i.e.,

$$\left[\frac{\rho_e U_e k}{\mu_e}\right]_{\mathrm{TR}}=200\left(\frac{T'}{T_e}\right)\left[1+350\left(\frac{k}{R_N}\right)\right] \tag{5b}$$

The two major differences between the Van Driest and PANT correlations are noted next. First, the wall-temperature-ratio dependence was moved from the disturbance parameter to the transition parameter. [Note that (T'/T_e) is an abbreviation for the denominator of the transition parameter term.] Second, the remaining term in the disturbance parameter (k/θ) was divided by $[1+350\,(k/R_N)]$ to approximately account for the stabilizing influences of surface curvature.

It can be seen from Eqs. (5) that the Van Driest formulation is equivalent to defining the existence of a critical roughness Reynolds number for transition; the value of this limiting Reynolds number, based on edge conditions and roughness height, is not constant however, but rather is a function of (T_w/T_e), M_e, and (k/R_N).

The present experimental conditions yielded $0.30 \leq (T'/T_e) \leq 0.55$ and $1.10 \leq (1+350\,\bar{k}/R_N) \leq 1.74$; according to Eqs. (5), these values dictate a rather broad regime for the critical roughness Reynolds number of transition, $66 \leq (\rho_e U_e \bar{k}/\mu_e)_{\mathrm{TR}} \leq 191$. However, in Fig. 8 it was shown that this parameter was well described, to within $\pm 20\%$, by a constant value of 106.

Figure 9 shows a comparison of present results with the Van Driest correlation. As was the case in PANT coordinates, the ballistics-range results showed a much stronger dependence of the transition parameter on the postulated disturbance parameter $(n=-1.62)$ vs that dictated by the wind-tunnel data $(n=-1.0)$. Once again, the two data sets exhibited a crossover in the regime of interest to re-entry applications.

One issue that bears further scrutiny is the "curvature correction" term, a factor which had its origins in the "trip" study of Ref. 13. Here, transition experiments were conducted on a hemispherical model with isolated spherical roughness elements placed in a row normal to the flow direction. The model was exposed to low Mach number $(M_\infty = 2.0)$ ideal-gas wind-tunnel environments; no heat-transfer or surface mass-transfer effects were present. Values of $[1+350\,k/R_N]$ ranged from 1.43 to 2.62.

Swigart,[27] in his analysis of the limited "pre-PANT" data base, discussed the validity of applying this curvature-

correction term to the problem of transition on blunt bodies with distributed roughness. As a minimum, it might be expected that the constant of 350 in the Van Driest correction would require modification. This term was applied[11] however, without modification, to both the PANT[5] data base [values of $(1+350\ k/R_N)$ ranging from 1.08 to 6.60] and to the subsequent Laderman[7] data base (values from 1.09 to 1.24).

In Fig. 10, all ballistics-range data were replotted in Van Driest coordinates without this curvature correction term being applied. A notable increase in the level of agreement between present data and the Van Driest formulation resulted, i.e., the ballistics-range data ($n=-1.23$) and the wind-tunnel data ($n=-1.0$) were somewhat reconciled in trends. While some may argue that such an "apples vs oranges" comparison is meaningless, given this "near reconciliation" of these two data sets the question then arises: why might this curvature correction be applied with some validity to the wind-tunnel data and apparently with less validity to the ballistics-range data?

In essence, the curvature-correction term reduces the physical roughness height of the surface to an effective roughness height by the product of $1/(1+350\ k/R_N)$. One inherent difference between the ballistics-range experiments and the vast majority of the wind-tunnel experiments was the presence of ablation. In Refs. 7 and 8 blowing was found to be a destabilizing influence; unfortunately, those wind-tunnel data obtained under the simultaneous conditions of surface roughness and blowing were not shown in comparison with the Van Driest formulation. One possibility that finds some credence in Fig. 10 (as well as in those comparisons to be shown in Sec. III, E) is that the destabilizing influence of surface mass transfer may effectively negate any stabilizing influences due to surface curvature. (Dirling[31] has hypothesized that "blowing changes the sign of the normal pressure gradient across the boundary layer, thus providing the destabilizing influence of blowing" generally noted.)

Obviously, such a comparison serves only to provide an indication that these competing mechanisms effectively counter one another under present test conditions. More thorough analyses of the Laderman[7]/Demetriades[8] data are called for, followed, perhaps, by further detailed experimentation, in order to better resolve this issue.

C. Bishop Correlations

Bishop[15] proposed a two-part formulation to the problem of defining mean transition-front locations on blunt bodies with distributed roughness. The nosetip flowfield was divided into "two distinct regions: a forward region where concave streamline curvature dominates transition, and a following region where streamline curvature is not an influence." It was reasoned that "flow passing through the near-normal portion of the (bow) shock must turn sharply to follow the body" and that the resulting "strong concave streamline curvature is thought to form streamwise (Goertler) vortices which are destabilizing and cause transition to occur earlier than would be predicted otherwise." Based on the available wind-tunnel data, the boundary between these two flow regions was sketchily defined by an (S/R_N) value of $\simeq 0.3$ in the $\simeq 5 \le M_\infty \le \simeq 8$ regime and an (S/R_N) value of $\simeq 0.4$ for $M_\infty \simeq 10$. These two regions are referred to here as the weak and strong curvature regions and will be discussed in that order.

Equations (6) summarize the weak curvature region correlation.

$$\frac{Re_{\theta,\mathrm{TR}}}{[1+4.5(T_w/T_e)M_e^2]^{1/2}_{\mathrm{TR}}} = 5.60\left[\frac{k}{2R_N}\right]^{-0.33} \tag{6a}$$

where,

$$(S/R_N) \ge \simeq 0.3 \quad \text{for} \quad \simeq 5 \le M_\infty \le \simeq 8 \tag{6b}$$

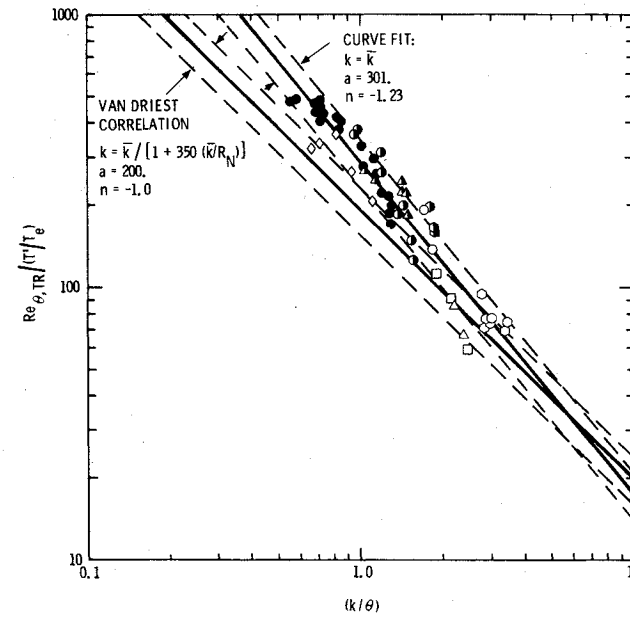

Fig. 10 Ballistics-range data without curvature correction vs Van Driest correlation.

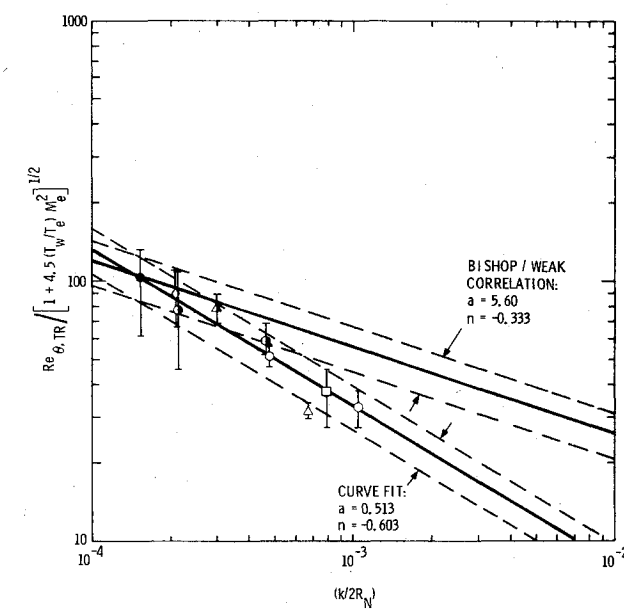

Fig. 11 Ballistics-range data vs Bishop/weak curvature region correlation.

and,

$$(S/R_N) \ge \simeq 0.4 \quad \text{for} \quad M_\infty \simeq 10 \tag{6c}$$

The disturbance parameter was chosen to be a nondimensionalized roughness $(k/2R_N)$, making it the only one of those discussed herein to explicitly contain no fluid-mechanic quantities. This selection was based on "the simple observation that the tripping effectiveness of a roughness element diminishes with the size of the body on which it is placed." The transition parameter can be seen to be quite similar to that utilized by Van Driest [recall Eqs. (5)].

A linear extrapolation of the weak curvature/strong curvature boundary requirement noted in Eqs. (6) to the $M_\infty = 14$ environments of the present experiments defined a boundary value for (S/R_N) of $\simeq 0.52$; thus, only 3 or 4 of the 56 measured transition locations reported herein were in the weak curvature region. Further extrapolation to environments typical of advanced, high-ballistic-coefficient, re-entry bodies $(M_\infty \simeq 20)$ showed that Eqs. (6) should not be applied

anywhere between the nosetip stagnation point and the sonic-line location, $(S/R_N) \simeq 0.7$. Based on these requirements, no agreement between present data and Eqs. (6) was expected, but the comparison was made anyway for completeness (see Fig. 11).

The form of the disturbance parameter $(k/2R_N)$ dictates that all values of the transition parameter for any given combination of nosetip material and nosetip radius fall along a vertical line. Consequently, the symbols shown in Fig. 11 represent the average of all measurements for each (k, R_N) combination, with vertical lines being used to show the maximum and minimum experimental values. The curve fit of the experimental results was accomplished using the 56 individual data points measured herein.

As can be seen in Fig. 11, the ballistics-range data showed a much stronger dependence $(n = -0.603)$ on the postulated disturbance parameter vs that dictated by the wind-tunnel results $(n = -0.333)$. Any conclusions, however, regarding the validity of extrapolating Bishop's two-part correlation to actual nosetip materials and environments must come from comparisons of present data with the strong curvature-region equations; these are listed later as Eqs. (7).

As in Eqs. (6), the disturbance parameter was defined to be $(k/2R_N)$. Curvature effects were incorporated into the transition parameter through the introduction of freestream Mach number, freestream Reynolds number, and the nondimensional arc-length (S/R_N).

$$\frac{(S/R_N)_{\mathrm{TR}}}{[(T_w/T_e)^{1.23} M_\infty/(Re_{\infty,D})^{0.6}]_{\mathrm{TR}}} = 12.97\left[\frac{k}{2R_N}\right]^{-0.51} \tag{7a}$$

where

$$(S/R_N) \leq \simeq 0.3 \quad \text{for} \quad \simeq 5 \leq M_\infty \leq \simeq 8 \tag{7b}$$

and

$$(S/R_N) \leq \simeq 0.4 \quad \text{for} \quad M_\infty \simeq 10 \tag{7c}$$

Solving Eqs. (7) for $(S/R_N)_{\mathrm{TR}}$ shows that, in the strong curvature region, transition location moves forward in proportion to $1/(Re_{\infty,D})^{0.6}$, other terms being constant, or essentially constant, throughout those flight regimes of interest to re-entry vehicles. Alternatively, combining nose-radii terms in Eqs. (7) shows that

$$(S/R_N)_{\mathrm{TR}} \propto (\rho_\infty U_\infty/\mu_\infty)^{-0.6} (R_N)^{-0.1} \tag{8}$$

or, for present experimental conditions,

$$(S/R_N)_{\mathrm{TR}} \propto (P_\infty)^{-0.6} (R_N)^{-0.1} \tag{9}$$

Such dependencies were not substantiated by present results.

Figure 12 shows a comparison of the ballistics-range data with Eqs. (7); experimental averages and extremes are represented as in Fig. 11. Here, as in Fig. 11, the ballistics-range results defined a negative exponent essentially double that dictated by the wind-tunnel results. Further, the parameters given in Eqs. (7) do not collapse present data to a reasonable band (say ±20%) about the least-squares curve fit. This is best illustrated by the $R_N = 3.18$ cm CMT data subset (20 points) which covers the entire transition-location regime of interest, from stagnation-point proximity to sonic-line proximity; for $(k/2R_N) = 1.53 \times 10^{-4}$, the transition parameter was found to range from $\simeq 600$ at the stagnation point to $\simeq 1800$ at the sonic line, a factor of 3 increase. The utility of such a correlating scheme for predicting transition location on re-entry vehicle nosetips must, therefore, be questioned.

D. Finson Correlation

Finson[14] was chartered by the U.S. Air Force in the mid 1970's to perform "a critical and independent evaluation of the (then) existing ground test (wind-tunnel) data on nosetip transition and of the transition criteria used for nosetip design." Further, he was to make a "determination of the manner in which the data base could be extended to provide a completely unambiguous definition of nosetip transition." His thorough analysis of the wind-tunnel data resulted in a reformulation of the problem in terms of an alternate correlation, summarized below by Eq. (10). He further noted, however, that "ballistics-range experiments with potential nosetip materials would be invaluable in bridging the gap between wind-tunnel tests and actual re-entry conditions."

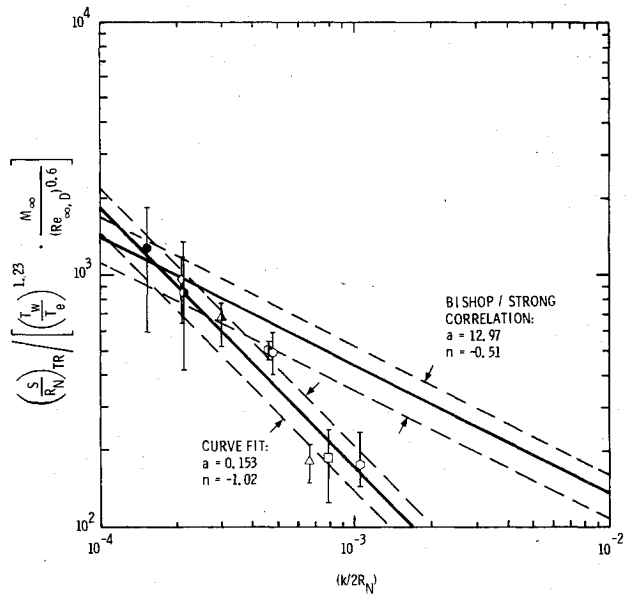

Fig. 12 Ballistics-range data vs Bishop/strong curvature region correlation.

$$\frac{Re_{\theta,\mathrm{TR}}}{[1 + (10^3\theta/R_N)]_{\mathrm{TR}} (\nu_w/\nu_e)^{1/2}_{\mathrm{TR}}} = 3.50 \times 10^5 \left[\frac{\rho_k U_k k}{\mu_k}\right]^{-1.64} \tag{10}$$

Definition of $(\rho_k U_k k/\mu_k)$ as a potential disturbance parameter had its origins in some of the early boundary-layer trip investigations, e.g., Smith and Clutter[24] and Van Driest et al.[12,13]

In Ref. 24 a correlation approach "involving $(\rho_k U_k k/\mu_k)$ was chosen because a Reynolds number is inferred as the critical parameter if it is assumed either that a wake is created or that vortices are shed from the roughness elements at a certain critical Reynolds number and that one or both of these disturbances either cause immediate transition or, when amplified, cause transition farther downstream." In summary,[24] it was reported that "the value of this critical Reynolds number (which first alters the smooth-wall transition location) was found to be substantially independent of all test variables except the shape of roughness." Further, "the value of the roughness Reynolds number necessary to move transition forward to the roughness itself was also determined for three types of roughness and was found to be approximately constant for a given type of roughness." When a narrow strip of sand-grain distributed roughness elements was used as the tripping device on a flat plate in low speed flows,[24] the value of the critical roughness Reynolds number to first affect boundary-layer transition was found to be $\simeq 250$ to $\simeq 300$, while values of $\simeq 400$ were required to bring transition to the trip location itself.

Calculations based on the model of Ref. 28 showed that the roughness Reynolds number was equal to the ratio of the rate at which fluctuation energy was produced by the roughness elements to the rate at which it was dissipated within the boundary layer.

It can be seen, therefore, that selection of a roughness Reynolds number term as the disturbance parameter is based on firm experimental and theoretical evidence. The one complication that arises, however, is the necessity to expand the predictive capabilities of existing nosetip shape-change codes to allow for the calculation of laminar boundary-layer profiles.

The transition parameter utilized by Finson was Re_θ based on edge conditions, modified for curvature and wall-temperature-ratio effects. It was noted that the kinematic viscosity $\nu = \mu/\rho$ varied significantly across the boundary layer and that a physically more realistic value to use would be one associated with "the middle of the layer." The modifying term $\sqrt{\nu_w/\nu_e}$ was therefore introduced to account for this effect, and, in essence, served to eliminate the wall-to-edge temperature-ratio dependence noted in the wind-tunnel data.

The other modifying term, $[1+10^3\theta/R_N]$, was introduced to account for the stabilizing influences of surface curvature; it was applied to the transition parameter rather than the disturbance parameter "based on the expectation that these factors should stabilize the boundary layer, that is, raise the value of Re_θ required for transition rather than reduce the effective roughness height."

Figure 13 shows a comparison of the ballistics-range data with Finson's correlation of the wind-tunnel data. The message is clear: the ballistics-range data were well described, to within $\pm 20\%$, by $(\rho_k U_k \bar{k}/\mu_k)_{TR} = 98.4 = \text{const}$. This value of $\simeq 100$ for the case of three-dimensional roughness elements distributed spatially over the entire test surface, was below those values of $\simeq 250$ to $\simeq 400$ defined by the finite-width sand-grain trip results of Smith and Clutter,[24] as would be expected.

The apparent validity of applying the concept of a constant (critical) roughness Reynolds number for transition to the ballistics-range data has thus been further substantiated (recall Fig. 8). The question remains, is there a variation of this correlating approach capable of reconciling these two independent nosetip-transition data sets?

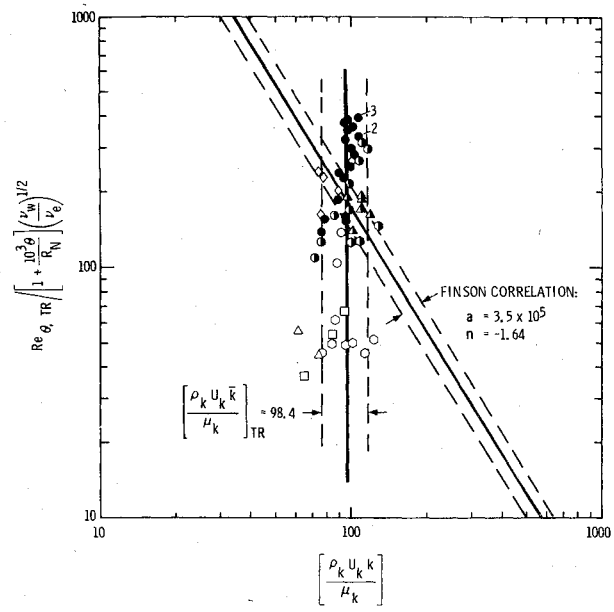

Fig. 13 Ballistics-range data vs Finson correlation.

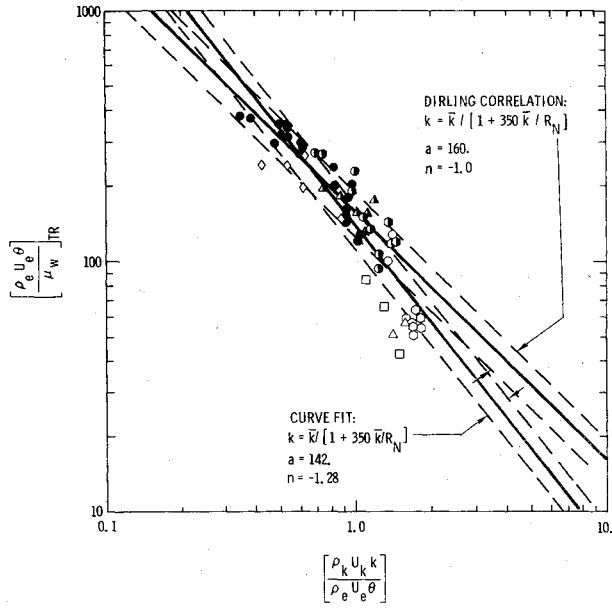

Fig. 14 Ballistics-range data vs Dirling correlation.

E. Dirling Correlation

Based on the same physical arguments discussed in the previous section (namely, that in the roughness-dominated regime, transition is caused by "the formation of vortices from the tips of the roughness elements"), Dirling[10] cast the PANT wind-tunnel data base[5] into a critical roughness Reynolds number framework. His formulation of the problem is summarized by Eqs. (11).

$$[\rho_e U_e \theta/\mu_w]_{TR} = 160[\rho_k U_k k/\rho_e U_e \theta]^{-1.0} \tag{11a}$$

i.e.,

$$[\rho_k U_k k/\mu_w]_{TR} = 160 = \text{const} \tag{11b}$$

where

$$[\rho_k U_k k/\mu_w] \geq 200 \quad \text{by } M_e = 1.0 \tag{11c}$$

and

$$k = \frac{\bar{k}}{[1+350(\bar{k}/R_N)]} \tag{11d}$$

The disturbance parameter was taken to be a relative roughness height (k/θ) modified by the ratio of fluid momentum at the top of the roughness elements to that which exists at the edge of the boundary layer. The roughness height k to be used in this parameter, as well as the height k at which the fluid density and velocity were to be calculated, was the average physical roughness height of the surface (here $\bar{k}$) reduced by the Van Driest term[13] $1/[1+350\ (\bar{k}/R_N)]$ to account for the stabilizing influences of surface curvature (recall the discussions of Sec. III, B). Surface mass-transfer effects on the laminar boundary-layer profile were also modeled, with U_k varying in direct proportion to the computed reduction in skin friction due to blowing.

The transition parameter was taken to be a Reynolds number based on fluid density and velocity at the edge of the boundary layer, the smooth-wall momentum thickness, and the fluid viscosity calculated at the wall temperature (i.e., at that temperature level reasoned to be most representative of the surface-roughness elements and the fluid in direct contact with them). A plot of the PANT wind-tunnel data in these coordinates can be found in Fig. 2 of Ref. 2.

Most importantly, it should be noted that this formulation is equivalent to stating that $(\rho_k U_k k/\mu_w)_{TR} = 160 = \text{const}$. The distribution of this roughness Reynolds number with (S/R_N) around the nosetip surface shows that it reaches a maximum value slightly ahead of the sonic-line location. The requirement that this roughness Reynolds number reach a maximum value of 200 by $M_e = 1.0$ was defined by the wind-tunnel results, i.e., when transition was observed to occur on the nosetip it was always located in the subsonic-flow region.

Figure 14 shows a comparison of the ballistics-range data with Dirling's correlation. A curve fit of present results yielded $a=142$, $n=-1.28$, i.e., the ballistics-range data and the wind-tunnel data were found to exhibit quite similar trends when plotted in these coordinates. In fact, the vast majority of all range data were found to be within $\pm 20\%$ of Dirling's correlation, the only notable discrepancies occurring under large $\bar{k}$, small R_N conditions.

Earlier comparisons of these two data sets in Van Driest coordinates had shown that the requirement to apply the curvature correction term $1/[1+350\bar{k}/R_N]$ to the mean roughness height $\bar{k}$ may be negated in those cases where mass addition (ablation) is present (recall discussions in Sec. III, B). A similar approach was applied here, wherein the ballistics-range data were retransformed into Dirling coordinates without the curvature-correction term being applied ($k=\bar{k}$). Results are shown in Fig. 15.

Plotted in this manner, the two data sets were found to exhibit identical trends ($n=-1.0$), i.e., both data sets were well described by $(\rho_k U_k k/\mu_w)_{TR}=\text{const}$. (Dirling's calculations were substantiated by those of Finson which yielded $a=186$, $n=-1.01$ in these coordinates.) Without the curvature correction term being applied to the range data, the value for this constant (critical) roughness Reynolds number for transition was 20% above that defined by the wind-tunnel data. Considering the complex differences between the range and tunnel experiments (nonuniform vs uniform roughness heights, blowing vs no blowing, real-gas vs ideal-gas environments, and quiescent vs nonquiescent environments) the success of this correlating approach in reconciling these two unique data sets was most encouraging.

In closing, the issue of extrapolating such a transition model to actual re-entry conditions must be addressed. For nosetip materials and environments of interest to re-entry applications, transition occurs in the roughness-dominated regime. The physical mechanism that dominates is the production of turbulence energy by the roughness elements through a vortex-shedding process, leading to a rapid breakdown of the laminar boundary-layer flow to a turbulent state once some critical Reynolds number has been exceeded (one example of what Morkovin[29] has often referred to as a "bypass mechanism"). The early tripping-effectiveness studies support this view,[24] Dirling's analysis of the PANT data supports this view,[10] and present results support this view. Further, in the present case, preablated carbonaceous nosetips were flown at hypersonic velocities in a ballistics range, the one ground-based facility that most closely simulates actual re-entry conditions. Given that the physics are correctly modeled, and that this modeling has been substantiated by experiments at conditions quite close to those experienced in the real-world flight regime of interest, then extrapolation of such a model to actual re-entry conditions seems justified.

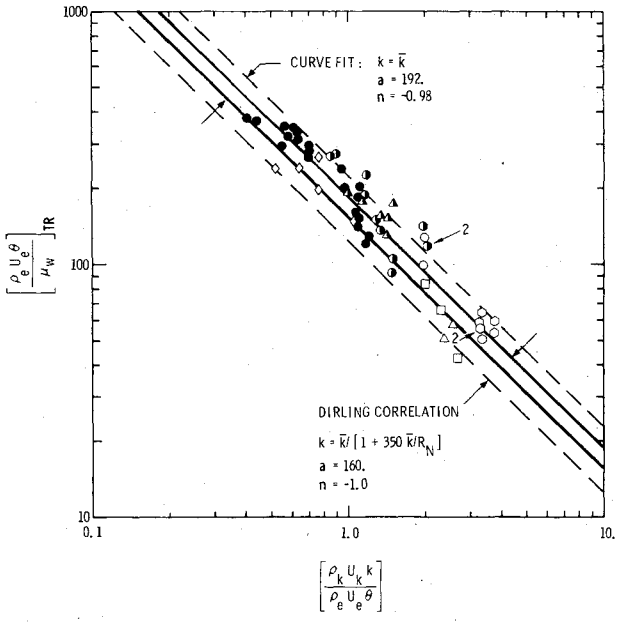

Fig. 15 Ballistics-range data without curvature correction vs Dirling correlation.

The one caveat that remains centers on the apparent competing mechanisms of surface curvature and mass addition. For re-entry calculations, if one feels compelled to use the Van Driest curvature-correction term to modify (reduce) $\bar{k}$ for materials of interest, then a value for $(\rho_k U_k k/\mu_w)_{TR}$ of order 150 should be used (recall Fig. 14). If one elects to use $k=\bar{k}$ (i.e., the average microroughness height for each graphitic material or the equivalent mean graphitic microroughness height for each composite material) then a value for $(\rho_k U_k k/\mu_w)_{TR}$ of order 200 should be used (recall Fig. 15).

IV. Conclusions

Results obtained from present ballistics-range nosetip-transition experiments, and comparisons of these results with correlations based on existing wind-tunnel data, led to the following conclusions:

1) Present experimental results were found to be well correlated within an established framework previously applied to analyses of transition data for flows over rough surfaces, namely, the concept of a constant (critical) roughness Reynolds number for transition. Dirling's correlation,[10] based on existing wind-tunnel data cast into this critical-roughness Reynolds-number framework, was the only correlation of those examined that could reconcile the ballistics-range and wind-tunnel results. Therefore, based on analyses of these two independent data sets, $[\rho_k U_k k/\mu_w]_{TR}=\text{const}$ best represents the physics of roughness-dominated transition on blunt bodies in hypersonic flows. Extrapolation of this correlation to actual re-entry materials and environments requires that conclusions 2 and 3 be addressed.

2) Orthogonal-weave composite nosetip materials tested under the present effort were found to possess equivalent mean graphitic microroughness heights double those values defined by the microscopy-measurement/composite-averaging technique. Application of the formerly noted correlation to any bulk graphite requires that k be set equal to the material's arithmetic average microroughness height, as defined by microscopy. However, application of this correlation to any composite/woven material requires that k be set equal to the material's equivalent mean graphitic microroughness height, as defined by experiment.

3) Due to the apparent competing influences of surface curvature (stabilizing) and surface mass transfer (destabilizing), a question has been raised concerning application of the Van Driest curvature-correction term[13] to the roughness height utilized in this correlation. Comparisons of present results (with ablation) vs the PANT wind-tunnel data[5] (without blowing) indicate that, if the curvature-correction term is applied, i.e., if, $k=\bar{k}/[1+350\bar{k}/R_N]$ then, $[\rho_k U_k k/\mu_w]_{TR}\cong 150$. If the curvature-correction term is not applied, i.e., if, $k=\bar{k}$ then, $[\rho_k U_k k/\mu_w]_{TR}\cong 200$.

References

[1] English, E. A., "Nosetip Recovery Vehicle Post-flight Development Report," Sandia Laboratories Tech. Rept. SAND75-8059, Jan. 1976.

[2] Dirling, R. B. Jr., "Asymmetric Nosetip Shape Change During Atmospheric Entry," AIAA Paper 77-779, June 1977; also *AIAA Progress in Astronautics and Aeronautics-Aerodynamic Heating and Thermal Protection Systems,* Vol. 59, edited by L. S. Fletcher, New York, 1978, pp. 311-327.

[3] Swain, C. E., "Aerodynamics of Reentry Vehicles with Asymmetric Nosetip Shape Change," AIAA Paper 77-782, 12th Thermophysics Conference, Albuquerque, N. Mex., June 1977.

[4] Hall, D. W. and Nowlan, D. T., "Aerodynamics of Ballistic Reentry Vehicles with Asymmetric Nosetips," AIAA Paper 77-701, 10th Fluid and Plasma Dynamics Conference, Albuquerque, N. Mex., June 1977.

[5] Anderson, A. D., "Passive Nosetip Technology (PANT) Program, Interim Report, Volume X, Appendix A: Boundary Layer Transition on Nosetips with Rough Surfaces," SAMSO-TR-74-86, Jan. 1975.

[6] Phinney, R. E. and Baltakis, F. P., "Influence of Roughness on Heat Transfer and Transition: ART Program Data Report," Naval Ordnance Laboratory Tech. Rept. NOLTR 73-231, Dec. 1974.

[7] Laderman, A. J., "Nosetip Transition Experimentation Program Final Report, Volume I," SAMSO TR 76-120, June 1976.

[8] Demetriades, A., "Nosetip Transition Experimentation Program Final Report, Volume II," SAMSO TR 76-120, July 1977.

[9] Demetriades, A., "Roughness-Induced Transition on a Blunt Body Simulated by a DeLaval Nozzle Throat," Ford Aerospace and Communications Corp. Rept. U-6496, Nov. 1978.

[10] Dirling, R. B. Jr., Swain, C. E., and Stokes, T. R., "The Effect of Transition and Boundary Layer Development on Hypersonic Reentry Shape Change," AIAA Paper 75-673, 10th Thermophysics Conference, Denver, Colo., May 1975.

[11] Van Driest, E. R., "Evaluation of PANT Transition Roughness Data and Transition Criterion," unpublished memo to SAMSO, Nov. 1975.

[12] Van Driest, E. R. and Blumer, C. B., "Boundary-Layer Transition at Supersonic Speeds: Roughness Effects with Heat Transfer," *AIAA Journal*, Vol. 6, April 1968, pp. 603-607.

[13] Van Driest, E. R., Blumer, C. B., and Wells, C. S. Jr., "Boundary-Layer Transition on Blunt Bodies-Effect of Roughness," *AIAA Journal*, Vol. 5, Oct. 1967, pp. 1913-1915.

[14] Finson, M. L., "An Analysis of Nosetip Boundary Layer Transition Data," AFOSR-TR-76-1106, Aug. 1976.

[15] Bishop, W. M., "Transition Induced by Distributed Roughness on Blunt Bodies in Supersonic Flow," AIAA Paper 77-124, 15th Aerospace Sciences Meeting, Los Angeles, Calif., Jan. 1977.

[16] Reda, D. C., Leverance, R. A., and Longas, S. A., "Aerothermodynamic Testing and Analyses of Reentry Vehicle Nosetips in Hypersonic Ballistics-Range Flight," 22nd International Instrumentation Symposium, Instrument Society of America, San Diego, Calif., May 1976.

[17] Reda, D. C. and Leverance, R. A., "Boundary-Layer Transition Experiments on Pre-Ablated Graphite Nosetips in a Hyperballistics Range," *AIAA Journal*, Vol. 15, March 1977, pp. 305-306.

[18] Reda, D. C. and Brown, H. S., "Analysis of Nosetip Boundary-Layer Transition Data Utilizing Interactive Graphics," 24th International Instrumentation Symposium, Instrument Society of America, Albuquerque, N. Mex., May 1978.

[19] Reda, D. C. and Raper, R. M., "Measurements of Transition-Front Asymmetries on Ablating Graphite Nosetips in Hypersonic Flight," *AIAA Journal*, Vol. 17, Nov. 1979, pp. 1201-1207.

[20] Reda, D. C., "Comparative Transition Performance of Several Nosetip Materials as Defined by Ballistics-Range Testing," 25th International Instrumentation Symposium, Instrument Society of America, Anaheim, Calif., May 1979; also *ISA Transactions*, Vol. 19, No. 1, 1980, pp. 83-98.

[21] Norfleet, G. D., Hendrix, R. E., and Jackson, D., "Development of a Hypervelocity Track Facility at AEDC," AIAA Paper 77-151, 15th Aerospace Sciences Meeting, Los Angeles, Calif., Jan. 1977.

[22] Rafinejad, D., Dahm, T. J., Brink, D. F., Abbett, M. J., and Wolf, C. J., "Passive Nosetip Technology (PANT II) Program: ABRES Shape Change Code (ASCC) Computer User's Manual," SAMSO-TR-77-11, Oct. 1976.

[23] Dirling, R. B. Jr., "On the Relation between Material Variability and Surface Roughness," AIAA Paper 77-402, *Proceedings of 18th Structures, Structural Dynamics and Materials Conference,* San Diego, Calif., March 1977.

[24] Smith, A.M.O. and Clutter, D. W., "The Smallest Height of Roughness Capable of Affecting Boundary-Layer Transition," *Journal of the Aero/Space Sciences*, April 1959, pp. 229-245, 256.

[25] Hama, F. R., "Boundary Layer Characteristics for Smooth and Rough Surfaces," *Transactions of the Society of Naval Architects and Marine Engineers*, Vol. 62, 1954, pp. 333-358.

[26] Reda, D. C., "Boundary-Layer Transition Experiments on Sharp, Slender Cones in Supersonic Freeflight," *AIAA Journal*, Vol. 17, Aug. 1979, pp. 803-810.

[27] Swigart, R. J., "Roughness-Induced Boundary-Layer Transition on Blunt Bodies," *AIAA Journal*, Vol. 10, Oct. 1972, pp. 1355-1356.

[28] Finson, M. L., "A Reynolds Stress Model for Boundary Layer Transition with Application to Rough Surfaces," Physical Sciences, Inc., TR-34, 1975; see also SAMSO-TR-76-0322, 1976.

[29] Morkovin, M. V., "Critical Evaluation of Transition from Laminar to Turbulent Shear Layers with Emphasis on Hypersonically Traveling Bodies," AFFDL-TR-68-149, March 1969.

[30] Reda, D. C, "Correlation of Nosetip Boundary-Layer Transition Data Measured in Ballistics-Range Experiments," Sandia National Laboratories Tech. Rept. SAND79-0649, Nov. 1979.

[31] Dirling, R. B. Jr., personal communication, June 1980.